Fluid Viscoelasticity Drives Self-Assembly of Particle Trains in a Straight Microfluidic Channel

Francesco Del Giudice,[1,*] Gaetano D'Avino,[2] Francesco Greco,[2] Pier Luca Maffettone,[2] and Amy Q. Shen[3]

[1] *Systems and Process Engineering Centre, College of Engineering, Swansea University, Fabian Way, Swansea SA1 8EN, United Kingdom*

[2] *Dipartimento di Ingegneria Chimica, dei Materiali e della Produzione Industriale,Universitá degli Studi di Napoli Federico II, Piazzale Tecchio 80, 80125 Naples, Italy*

[3] *Micro/Bio/Nanofluidics Unit, Okinawa Institute of Science and Technology Graduate University, 1919-1 Tancha, Onna-son, Kunigami-gun, Okinawa 904-0495, Japan*

(Received 24 September 2018; revised manuscript received 6 November 2018; published 26 December 2018)

Strings of equally spaced particles (particle train) are tremendously important in a variety of microfluidic applications. By using inertial microfluidics, particle trains can be formed near the channel walls. However, the high particle rotation and large local shear gradient near the microchannel walls can lead to blurred images and cell damage, thus negatively affecting applications related to flow cytometry. To address this challenge, we demonstrate that adding a tiny amount of hyaluronic acid biopolymer to an aqueous suspension drives self-assembly of a particle train on the centerline of a square-shaped straight microchannel, with a throughput up to approximately 2400 particles/s. The fraction of equally spaced particles increases by increasing the volumetric flow rate and the distance from the channel inlet. Numerical simulations corroborate the experimental observations and, together with a simple qualitative argument on the particle train stability, shed insights on the underlying mechanism leading to particle ordering.

DOI: 10.1103/PhysRevApplied.10.064058

I. INTRODUCTION

Controlling the spacing between particles and cells at the micron-size level, hereafter particle or cell ordering, dramatically impacts a variety of applications, ranging from biomedical engineering to material science. Particle and cell ordering is essential in applications such as flow cytometry [1–3], cell separation [4], particle encapsulations [5,6], and fabrication of microfluidic particles or droplet crystals [7–9]. In material science, optical and acoustic properties of metamaterials can be tuned by the spatial composition of particles [10,11]. In tissue engineering, the local arrangement of cells (cell architecture) is a crucial parameter for the design of three-dimensional (3D) scaffolds [12] or printed tissues [13].

Particle trains (strings of ordered particles) organized on multiple streamlines were first observed by Segré and Silberberg [14], by using the inertial focusing principle. In their work, they employed particles with diameters in the range of $0.32 < d < 1.7$ mm suspended in a 1,3-butanediol and water mixture. They argued that the train formation was due to particle-particle hydrodynamic interactions. Matas *et al.* [15] observed trains of 425 and 825 μm particles organized on multiple streamlines of a tube with an 8-mm diameter. They ascribed the formation of trains to the coupling of particle-particle hydrodynamic interactions and inertial forces, as also theoretically proposed later by Lee *et al.* [7]. Di Carlo *et al.* [16] achieved particle trains on multiple streamlines in a square-shaped microchannel with a height of 50 μm. In their work, they employed particles with a diameter in the range of $4 < d < 20$ μm suspended in water, at a concentration range of $0.1 < \phi < 1$ vol %. Single-line particle and cell trains have been obtained by employing inertial microfluidics in a curved 50-μm channel [1] and in a straight channel with multiple nonrectangular cross sections [17]. However, in both cases, particle or cell trains were observed near the channel walls, where the particle or cell rotation and the local shear gradient are large. Large particle or cell rotation may lead to blurred images in cytometry applications that use line-scan-based interrogation, as reported by Goda *et al.* [18]. In addition, high local shear gradients may result in damaging delicate cells. Hence, particle trains should develop on the channel centerline, where both particle or cell rotation and local shear gradient are minimal.

Recently, the addition of polymer to aqueous suspensions was found to promote transversal migration of suspended particles toward the centerline of a straight

*francesco.delgiudice@swansea.ac.uk

microchannel [19–21], due to internal viscoelastic forces [22]. However, the majority of existing studies [23–25] dealing with particles in viscoelastic fluids flowing in microchannels have only considered very dilute suspensions (volume particle concentration lower than 0.1%). Hence, particles essentially behave as isolated objects and, upon alignment, the interparticle distances are so large that particle-particle hydrodynamic interactions can be considered negligible. To the best of our knowledge, very few works have examined the flow of suspension at higher particle concentrations. Xiang *et al.* [26,27] found that particles suspended in a near-constant-viscosity liquid at $\phi = 0.5$ vol % were focused on a single streamline in a curved 50-μm square-shaped microchannel, but did not display any ordered structure. For a similar suspending liquid, Kang *et al.* [28] found that particles with $5 < \phi < 10$ vol % segregated around the centerline of a straight 50-μm microchannel without forming particle trains. D'Avino *et al.* [29] employed numerical simulations to study the effect of viscoelasticity-mediated particle-particle hydrodynamic interactions on the spacing between pairs and triplets of particles suspended in a viscoelastic liquid with shear-thinning properties, at the centerline of a pressure-driven channel flow. They found that, in strongly shear-thinning elastic fluids, the distances between three aligned particles increase up to a value such that the particles behave like isolated objects. In the case of a multiparticle system, such repulsion dynamics might potentially lead to equally spaced structures. However, the limitation to only three particles remains; thus, it is still uncertain whether particle trains can be effectively achieved. So far, neither experimental nor numerical evidence of particle trains in viscoelastic liquids has been reported. It should also be emphasized that shear-thinning liquids have always been considered detrimental for particle alignment, since particles tend to migrate toward the channel walls [30,31]. Only very recently, Del Giudice *et al.* [32] showed that moving particles can be aligned on the centerline of a straight square-shaped microchannel, even in a shear-thinning liquid, by increasing the ratio of the particle size to the channel height. Therefore, further investigation on viscoelastic particle ordering seems in order.

In this work, we demonstrate that simple addition of a 1-wt-% hyaluronic acid biopolymer to an aqueous suspension drives self-assembly of single-line particle trains on the centerline of a squared-shaped straight microchannel. Particles with diameter $d = 20$ μm first align and then self-order on the centerline of the glass microchannel, with channel height $H = 100$ μm, and with a throughput up to approximately 2400 particles/s. Our results demonstrate that shear-thinning of the suspending liquid is in fact advantageous to achieve viscoelastic particle ordering. Numerical simulations corroborate the experimental observations and, together with a simple qualitative argument on the particle train stability, shed insights on the underlying mechanism leading to particle ordering.

II. METHODS

A. Preparation and characterization of the suspensions

We employ two solutions of hyaluronic acid (HA, molecular weight $M_w = 900$ kDa, Sigma Aldrich) at mass concentrations of 1 and 0.1 wt % in phosphate buffer saline (PBS, Sigma Aldrich, Japan). HA 1 wt % is prepared by adding polymer powder to MilliQ water at room temperature, and the solution is shaken vigorously to allow dissolution of the polymer. HA 0.1 wt % is prepared by diluting ten times the HA 1 wt % solution with PBS. Glycerol at 25 wt % (Nacalai, Japan) is subsequently added to HA 0.1 wt % to prevent particle sedimentation. Glycerol is not needed for the premixed HA 1 wt %, due to the high viscosity of the fluid. Polystyrene particles (Polysciences Inc.) 20 μm in diameter are added to both polymer solutions at volume concentrations $\phi = 0.3\%$, $\phi = 0.6\%$, and $\phi = 1\%$. The addition of particles to HA 1 wt % requires multiple steps of mixing due to the high viscosity of the solvent. No surfactant is used to enhance dispersion. Both suspensions are filtered by a standard 40-μm filter to remove potential aggregates.

Rheological measurements are carried out on a stress-controlled rheometer (Anton Paar MCR 502) with a stainless steel cone and plate geometry (50 mm in diameter, 1° angle). A solvent trap is used to avoid fluid evaporation. The temperature is kept constant at $T = 22$°C.

B. Microfluidic device

The inlet to the glass channel is fabricated of polymethylmethacrylate (PMMA, substrate thickness 1 mm, Kuraray Co. Japan), using a micromilling machine [33] (Minitech CNC Mini-Mill). Fabrication is carried out using 300- and 200-μm tips. The channel depth is kept constant at 200 μm. Finally, a hole is made to allow pumping of the suspension. The inlet to the glass channel is bonded on another PMMA substrate by immersing the two pieces in absolute ethanol (Sigma-Aldrich) for 20 min. The two PMMA pieces are then put on a hot press (Imoto IMC-180C, Japan) with plate temperature $T = 40°$ and pressure $\Delta P = 0.4$ MPa for 20 min (ΔP is the difference between the final pressure and the pressure detected when the hot plates touched the two PMMA pieces). A square-shaped glass microchannel (Vitrocom) with an internal height of $H = 100$ μm and external height of 200 μm is glued directly to the PMMA inlet.

C. Experimental procedure

The fluid is pumped at several volumetric flow rates Q using a high-precision Harvard PHD-Ultra syringe pump. We use Hamilton gas-tight glass syringes to avoid wall

deformation from affecting the rate of fluid delivery into the microchannel.

First, we impose $Q = 10$ μl/min for 10 min to allow flow stabilization. After flow stabilization, images are recorded using a high-speed camera (Phantom Miro M310, Vision Research). Since HA is expensive, images at higher Q are acquired as follows. The flow rate is kept to $Q = 10$ μl/min for 10 min, and then a higher flow rate is imposed. After 30 s, images are recorded and the flow is subsequently reset to $Q = 10$ μl/min. This procedure is not expected to bias our analysis. Indeed, the volume of the whole glass channel is $H \times H \times L = 0.1 \times 0.1 \times 100 = 1\ \text{mm}^3 = 1\mu\text{l}$. For $Q = 20$, $Q = 50$, and $Q = 100$ μl/min, the volume of fluid that flows through the channel after 30 s is 10, 50, and 100 μl, respectively, always higher than 1 μl. Therefore, during image acquisition, the sample is always fresh.

D. Determination of the distance between the particles

Particles from 1500 acquired images are tracked using a freely available particle-tracking subroutine for IDL (Harris Geospatial Solution) [34]. When two particles are in contact, the subroutine is unable to distinguish between the two particles; thus, they are treated as a single one. Bigger aggregates, instead, are disregarded from the analysis. The spacing between particles Δz is evaluated using a homemade subroutine for *Mathematica* (Wolfram) and then normalized by the particle diameter d. Histograms are then evaluated using ORIGIN Pro 2017, with binning size equal to d. The two boundary ends are set to 0 and 30 d.

III. RESULTS AND DISCUSSION

A. Experiments

Particle ordering in a straight microchannel is studied experimentally by suspending 20-μm polystyrene particles in a PBS solution containing 1 wt % HA at three particle loadings: $\phi = 0.3$, $\phi = 0.6$, and $\phi = 1$ vol %. To avoid particle clogging, we design a multicontraction inlet made of polymethylmethacrylate [the gray device in Fig. 1(a)]. The square-shaped glass microchannel with internal height $H = 100$ μm and total length $L = 10$ cm is glued inside the multicontraction inlet. A glass channel is preferred over the most commonly used polydimethylsiloxane (PDMS) since it is more rigid and, therefore, prevents channel deformation at high flow rates (channel deformation can affect the transversal migration of particles [36]).

Results from different experimental conditions are quantified through the Deborah number De, which is the ratio between the characteristic time λ of the fluid and the characteristic time t_f of the flow. The Deborah number can also be regarded as a characteristic ratio between elastic and viscous forces in flow conditions; whichever interpretation is adopted, the Newtonian liquid corresponds to $\text{De} = 0$, whereas $\text{De} > 0$ implies a certain degree of elasticity of the fluid. For a channel with a square cross section, the Deborah number is defined as

$$\text{De} = \frac{\lambda}{t_f} = \frac{\lambda Q}{H^3}, \tag{1}$$

where Q is the volumetric flow rate. In our experiments, the range of the Deborah number investigated is $6.2 < \text{De} < 62$, corresponding to the volumetric flow rate of $10 < Q < 100$ μl/min.

1. Hyaluronic acid 1 wt % in PBS drives formation of particle trains

Previous works highlighted that the rheology of the suspending liquid would affect the focusing dynamics of the flowing particles [23,24,37]. HA 1 wt % in PBS displays an almost constant shear viscosity η up to a shear rate of $\dot{\gamma} \sim 10\ \text{s}^{-1}$, followed by a shear-thinning behavior (shear viscosity η decreases with increasing shear rate) as $\dot{\gamma}$ increases [Fig. 1(b)]. The elasticity of the solution is quantified through the longest relaxation time λ and evaluated from the measurement of the storage modulus G' and the loss modulus G'' [see the inset of Fig. 1(b)]. Following a standard rheological procedure (i.e., small angle oscillatory shear) [35], we obtain $\lambda = 37$ ms from the intersection of the dashed and the dashed-dotted lines fitting the data at low frequencies. In summary, a PBS solution containing 1 wt % HA exhibits flow-dependent shear viscosity η and elastic properties quantified by $\lambda = 37$ ms.

The experiments are first performed for a suspension at a particle concentration $\phi = 0.6$ vol % in PBS containing 1 wt % HA. At a fixed distance from the inlet $L_z/H = 800$ ($L_z = 8$ cm), around 18 particles are visible within the observed portion of the channel $L_{\text{obs}} = 60d = 1.2$ mm [see the left panel of Fig. 1(c)]. As the Deborah number is increased, an increasing fraction of particles become progressively equally spaced, i.e., ordered. From a simple geometrical argument [see Eq. (2) below], 18 particles along L_{obs}, if ordered, should be spaced with a distance between their centers $s_{\text{theo}} = L_{\text{obs}}/18 \sim 3.3\ d$ (in dimensionless terms, $s^*_{\text{theo}} = s_{\text{theo}}/d = 3.3$). We indeed observe a dominant peak in the histograms at a dimensionless distance $s^* = 3.5$, in good agreement with the geometrical value. The peak of the distance distribution at $s^* = 3.5$ is also found to be independent of the Deborah number [Fig. 1(c)]. Interestingly, the fraction f of ordered particles with $s^* = 3.5$ is found to double from $f \sim 0.2$ at $\text{De} = 6.2$ ($\dot{\gamma} \simeq 170\ \text{s}^{-1}$) to $f \sim 0.4$ at $\text{De} = 62$ ($\dot{\gamma} \simeq 1700\ \text{s}^{-1}$). We experimentally verify that about 70% of the measured distances falls between $s^* = 3.5$ and $s^* = 5$, both for $\text{De} = 31$ and $\text{De} = 62$ [see the right panel of Fig. 1(c) and Videos S1 and S2], with a throughput (particle concentration ×

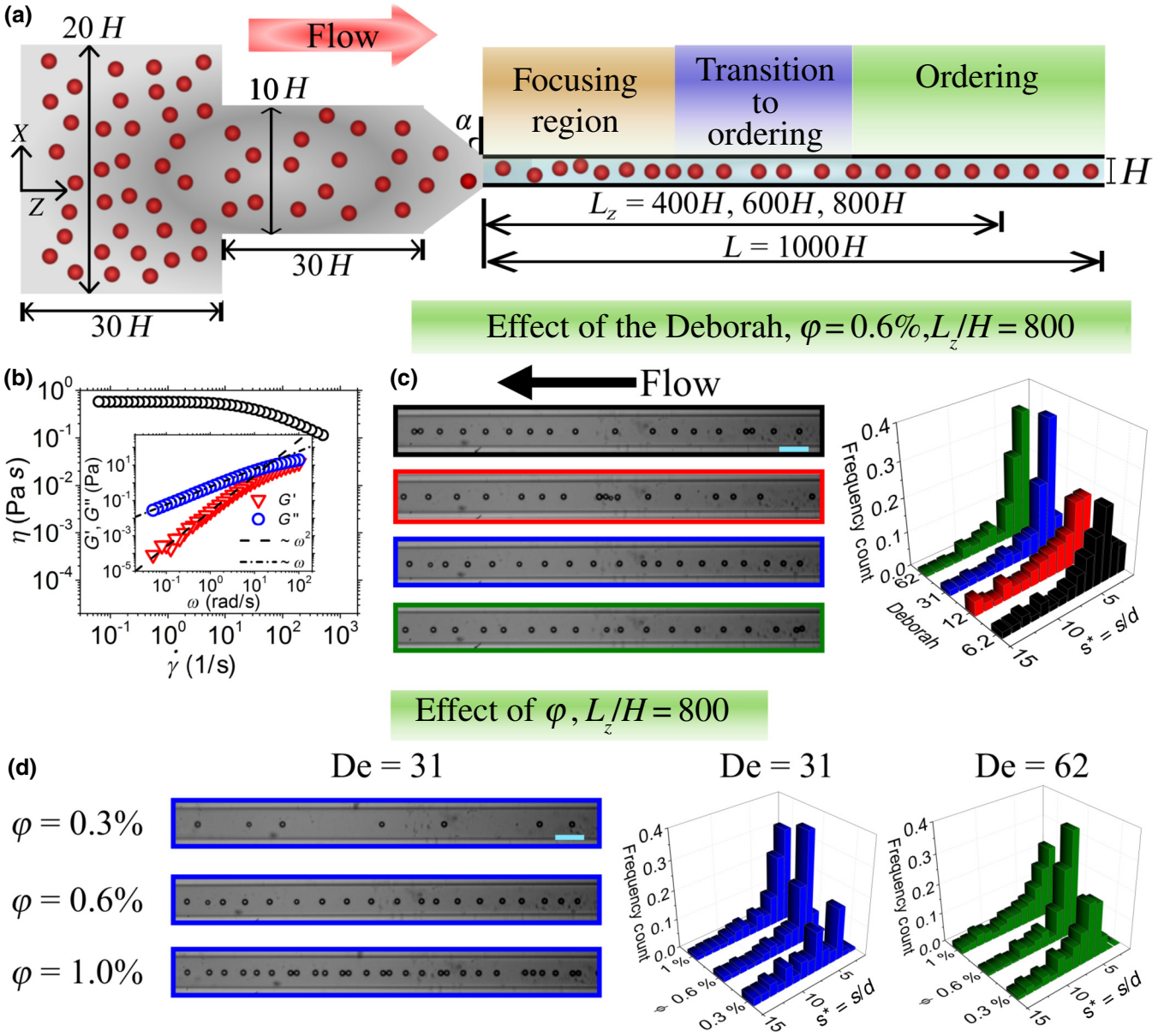

FIG. 1. Fluid viscoelasticity drives the self-assembly of particle trains in a straight microfluidic channel. (a) Schematic of the employed device with relevant dimensions. Particles converge gently to the glass channel, align after a certain length, and then self-order. The channel side is $H = 100$ μm and the angle is $\alpha = 70°$. Dimensions are not to scale. The device in gray is a multicontraction inlet made of polymethylmethacrylate. This design prevents particle clogging at the entrance of the glass microchannel (light blue rectangle). (b) Shear viscosity η as a function of the shear rate $\dot{\gamma}$ for hyaluronic acid (HA) at 1 wt % in PBS. The fluid displays a clear shear-thinning behavior above $\dot{\gamma} \sim 10$ s^{-1}. The inset shows the elastic modulus G' and the viscous modulus G'' as a function of the angular frequency ω for an imposed deformation $\gamma = 5\%$. The longest relaxation time $\lambda = 37$ ms is evaluated as the intersection between the dashed and the dashed-dotted lines, identified as the so-called "terminal region" [35]. (c) Higher Deborah numbers $\mathrm{De} = \lambda Q/H^3$ (Q is the volumetric flow rate) enhance the fraction of particles ordered at $s/d \sim 3.5$, where $d = 20$ μm is the particle diameter. Experimental snapshots at different De are also shown (using the same color code as the histograms). The flow is from right to left. The volumetric particle fraction is $\phi = 0.6\%$. (d) Particle ordering occurs at volumetric particle concentrations $\phi > 0.3\%$. At $\phi = 1\%$, an increasing number of "doublets" of particles is observed. The scale bar is 100 μm.

volumetric flow rate) of approximately 1200 particles/s (De = 31) and approximately 2400 particles/s (De = 62).

In the case of inertial ordering, the distance between the particles depends on the particle Reynolds number $\mathrm{Re}_p = \mathrm{Re}\,\beta^2$, where $\mathrm{Re} = \rho Q/\eta H$ is the Reynolds number, with ρ the fluid density, and $\beta = d/H$ is the confinement ratio [7]. Kahkeshani *et al.* [38] observed an average spacing $s^* = 5$ for $\mathrm{Re}_p = 2.8$ and $s^* = 2.5$ for $\mathrm{Re}_p = 8.3$.

In our experiments, however, we do not observe any Reynolds-dependent spacing; notice that our highest particle Reynolds number is $\mathrm{Re}_p = 0.0027$ (at De = 62); thus, inertial effects are always negligible.

As stated above, particle ordering stems from hydrodynamic interactions that become relevant when the particles are sufficiently close to each other [7,15,29,39]. Hence, particle concentration is an important parameter for the ordering mechanism. We then evaluate the spacing s^* at $L_z/H = 800$ as a function of the volumetric particle concentration ϕ for De = 31 and De = 62 [Fig. 1(d)]. At $\phi = 0.3$ vol %, the interparticle distances are quite large and random and no clear ordering can be detected [see the top snapshot in Fig. 1(d)], suggesting that hydrodynamic interactions in such conditions are weak. At $\phi = 0.6$ vol %, the highest ordering efficiency is found for both De = 31 and De = 62 [Fig. 1(d)]. By further increasing the particle concentration to $\phi = 1$ vol % [see the bottom snapshot of Fig. 1(d) and Video S3], we observe sequences of equally spaced particles with some occasional "doublets" or (less frequently) "triplets" of particles. Note that doublets of particles were not observed in the inertial ordering by Kahkeshani *et al.* [38]. Insights on the occurrence of doublets in viscoelastic self-assembly will be discussed in a later section.

2. Particle trains are not observed in a near-constant viscosity liquid

To test the effect of the shear thinning on particle ordering, we carry out the same experiments for a hyaluronic acid solution 0.1 wt % in PBS with the addition of 25 wt % of glycerol to prevent particle sedimentation. Different from the HA 1 wt % used previously, the HA 0.1 wt % has a constant shear viscosity η in the whole range of shear rate $\dot{\gamma}$ investigated [Fig. 2(a)]. The relaxation time evaluated from the intersection of the dashed and the dashed-dotted lines fitting the data at low frequencies [inset of Fig. 2(a)] is $\lambda = 32$ ms, which is very similar to the relaxation time of the HA 1 wt %.

At $L_z/H = 800$, despite varying both Deborah numbers (De = 26 and De = 52) and particle concentration ($\phi = 0.3$, $\phi = 0.6$, and $\phi = 1$ vol %), we do not observe particle ordering [Figs. 2(b) and 2(c)]. Interestingly, we notice the presence of sporadic "strings" of several very close particles, with few isolated particles between them, at both $\phi = 0.6$ vol % and $\phi = 1$ vol % [experimental snapshots are shown in Fig. 2(c)]. Such strings are not observed for particles suspended in HA 1 wt %, where only doublets of particles are found mainly at $\phi = 1$ vol %. We also find that the number of particle strings in HA 0.1 wt % increased at $\phi = 1.5$ vol % (Video S4 for De = 31 and Video S5 for De = 62). The formation of these strings can again be ascribed to the existence of the critical interparticle distance discussed above. D'Avino *et al.* [29] reported that the

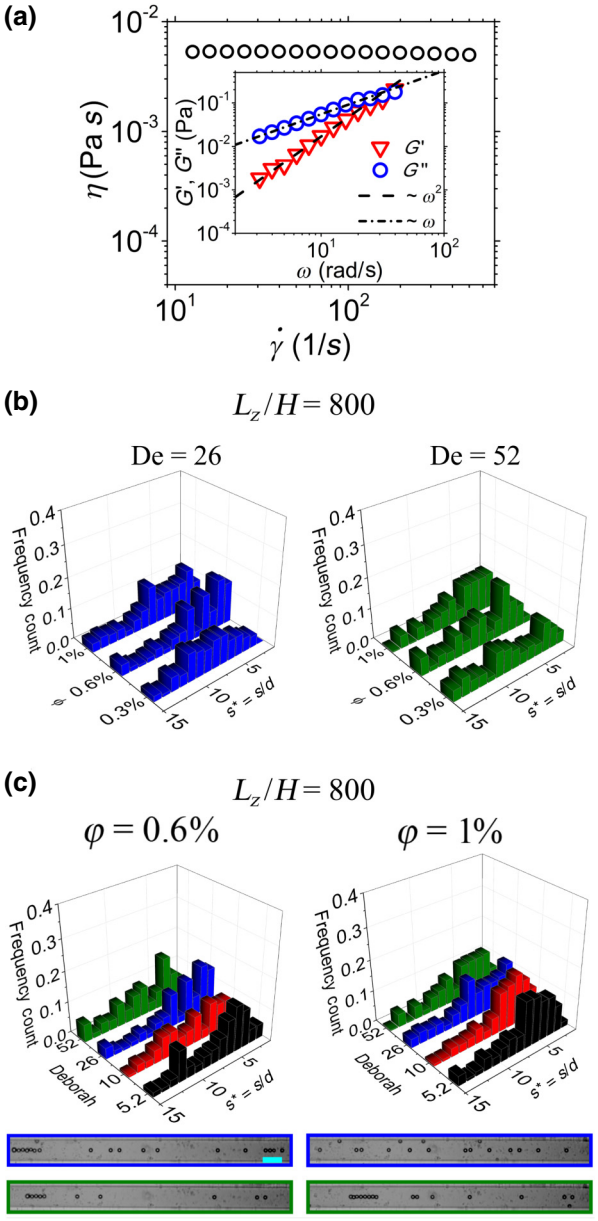

FIG. 2. Particle trains are not observed in a near-constant viscosity liquid. (a) Shear viscosity η as a function of the shear rate $\dot{\gamma}$ for hyaluronic acid (HA) at 0.1 wt % in PBS with the addition of 25 wt % of glycerol. The fluid has near-constant viscosity in the whole range of shear rates $\dot{\gamma}$ investigated. The inset shows the elastic modulus G' and the viscous modulus G'' as a function of the angular frequency ω for an imposed deformation $\gamma = 5\%$. The longest relaxation time $\lambda = 32$ ms is evaluated as the intersection between the dashed and the dashed-dotted lines (who identify the so-called terminal region [35]). (b) Effect of particle concentration ϕ on the normalized distance between the particles $s^* = s/d$ at two different Deborah numbers De = 26 and De = 52. Particle ordering is not observed in any of the conditions reported. (c) Deborah number $\mathrm{De} = \lambda Q/H^3$ (Q is the volumetric flow rate) does not affect significantly the distance between the particles s^*, at two different volume concentrations $\phi = 0.6\%$ and $\phi = 1\%$. The scale bar is 100 μm.

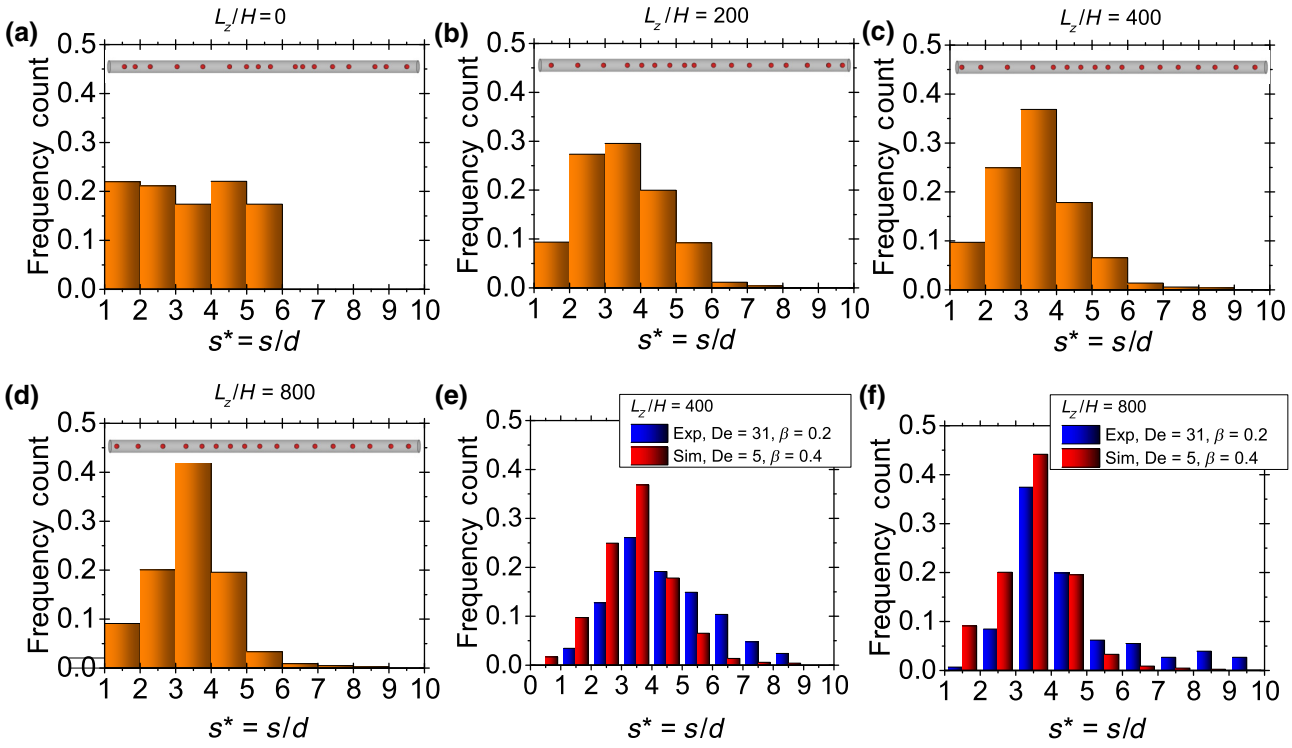

FIG. 3. Numerical simulations are in good agreement with experiments. (a)–(d) Normalized distances between particles s^* at several distances from the channel inlet L_z/H. Screenshots from simulations are included as an inset in each panel (full videos are available as Videos S6–S10). Particles at $L_z/H = 0$ are already aligned at the channel inlet. (e),(f) Comparison between experimental and numerical distributions of s/d at $L_z/H = 400$ (e) and $L_z/H = 800$ (f). The experimental distributions are evaluated at De = 31 and $\beta = 0.2$, while the numerical simulations are carried out at De = 5 and $\beta = 0.4$ (see the main text for more details on the choice of the parameter values in the simulations).

value of such a distance increases as the amount of shear-thinning decreases; i.e., particle attraction is enhanced in a near-constant-viscosity liquid, corroborating our experimental evidence. Finally, notice that inertial effects are also expected to be negligible in this case, as the highest particle Reynolds number is $\mathrm{Re}_p = 0.03$ (at De = 62).

B. Numerical simulations

We investigate the particle-ordering mechanism through numerical simulations (Fig. 3) by considering that all the particles are aligned along the centerline when entering the channel [40–48].) We face three main difficulties: the large number of particles of the experiments cannot be dealt with by direct numerical simulations, the imposed De values are out of reach of computations (because of numerical instabilities), and the experimental confinement ratio $\beta = 0.2$ cannot be simulated because the relative velocities between the particles turn out to be very small and comparable with the numerical accuracy.

The first issue is tackled in the following way. Direct numerical simulations are used to calculate the relative velocities of a three-particle system for several initial interparticle distances. The selected distances between the particles and the corresponding computed interparticle velocities are then used to model the multiparticle system, with the assumption that each particle in the train hydrodynamically interacts only with its trailing and leading spheres. In this way, the particle train dynamics can be computed by solving a simple set of ordinary differential equations [40]. The direct numerical simulations of the three-particle system are performed by choosing a two-mode Giesekus constitutive equation that accurately matches the HA 1 wt % in PBS rheology [40].

The second and third issues are, in fact, solved together by noting that, as reported by D'Avino *et al.* [29], for a system of two particles suspended in Giesekus fluid, the relative particle velocity scales approximately as $\mathrm{De}\,\beta^3$. Based on this scaling, we simulate at De = 5 and $\beta = 0.4$ to describe the experimental situation with De = 32 and $\beta = 0.2$. The predicted dimensionless interparticle distances s^* at several distances from the inlet L_z/H are reported in Fig. 3.

1. Comparison of simulation predictions with experiments

We first evaluate numerically the distributions of the interparticle distances at increasing distances from the

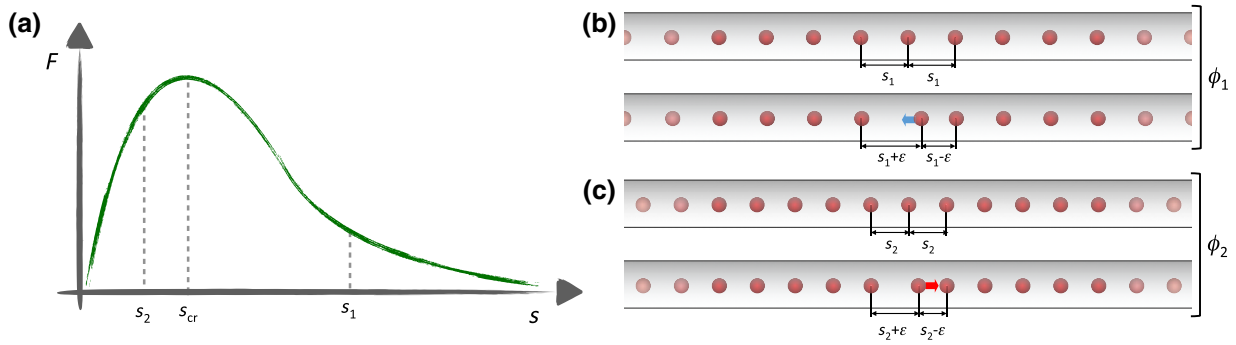

FIG. 4. A stability analysis based on pairwise interactions supports the experimental and numerical results. (a) Sketch of the effective repulsive force between two particles in a viscoelastic fluid (see text) for a sufficiently high Deborah number. (b) A train of equally spaced particles is formed at some volume fraction ϕ_1 corresponding to a distance $s_1 > s_{cr}$. A particle of the train displaced by a small amount ϵ experiences two different repulsive forces from the trailing (at distance $s_1 + \epsilon$) and the leading (at distance $s_1 - \epsilon$) sphere. Since s_1 is in the branch where the force $F(s)$ has a negative slope, the force between the displaced particle and the leading one is lower than the force between the particle and the trailing sphere. The net force is, then, toward the trailing sphere (blue arrow) and the interparticle distances are restored to the original value s_1. (c) The same scenario as in panel (b), where the volume fraction is $\phi_2 > \phi_1$ and the interparticle distance is $s_2 < s_{cr}$. Now, the force between the displaced sphere and the leading one is higher than the force between the particle and the trailing sphere. Thus, the displaced sphere moves toward the leading one and a pair is formed.

channel inlet [Figs. 3(a)–3(e)]. At $L_z/H = 0$ (channel inlet), particles are uniformly distributed within the range $1 < s^* < 6$ [Fig. 3(a) and Video S6]. As L_z/H increases, a clear peak at $s^* = 3.5$ is observed, in good agreement with experiments [Figs. 3(c)–3(d) and Videos S9 and S10]. The comparison between the numerical distributions at increasing distances L_z/H also shows that the ordering dynamics is quite fast close to the entrance, but slows down at long distances from the inlet (the distribution at $L_z/H = 400$ looks very similar to that at $L_z/H = 800$).

It should again be remarked that the experiments show the general tendency to assemble trains of particles, but also show the presence of paired particles in doublets, intercalating ordered strings. This presence is more frequent as the particle loading increases [see Fig. 1(d)]. A similar trend is clearly visible also in the simulations (Videos S6–S10), thus confirming the qualitative good agreement between numerics and experiments.

We also compare the numerical distributions of s^* with the experimental ones, both at $L_z/H = 400$ and $L_z/H = 800$ [red and blue bars in Figs. 3(e) and 3(f), respectively]. The simulations slightly overestimate the peak as compared to experiments, especially at $L_z/H = 400$. This result is not surprising as, in the numerical simulations, the particles enter the channel prealigned, in contrast with the experimental conditions (a random distribution over the channel inlet cross section). However, a good qualitative agreement between the two distributions is observed, suggesting that the scaling with De and β proposed by D'Avino *et al.* [29] is reasonable. Taken together, these results show that the confinement ratio β, the Deborah number De, and the channel length L_z provide some freedom of tuning to achieve particle ordering in different flow conditions. As a final note, we also try to perform experiments at $\beta = 0.4$. In this case, however, we observe significant clogging within the glass channel.

C. Viscoelasticity-induced effective repulsive force leads to ordering or pairing in particle trains

A simple qualitative argument can be used to justify the observed formation of trains of equally spaced particles in confined viscoelastic flows. We start from the assumption that the particles move "caged" at the channel centerline by the normal stresses arising in a viscoelastic flow [23]. We then examine the stability of the train arrangement, by slightly perturbing its one-dimensional (1D) crystal-like configuration. To keep the analysis simple, we also assume that a generic particle in the train interacts (hydrodynamically) with only the two nearest neighbors. As shown in Fig. 7 of Ref. [29], for De larger than some critical value De_{cr} (its exact value depending on confinement ratio and fluid rheology), two particles display a velocity difference that makes them separate from each other, as if they were subjected to a repulsion force $F(s)$. This repulsive force $F(s)$ at large De values (as in our experiments) is nonmonotonic and presents a maximum at a critical interparticle distance s_{cr}. A qualitative sketch of the force versus distance curve is depicted in Fig. 4(a), which is drawn by analogy with the results of direct numerical simulations reported in Ref. [29] for a relatively high value of the Deborah number. A simple stability argument gives the following conclusions. If the train spacing is larger than s_{cr}, say, s_1, a local small perturbation ϵ of the position of a particle generates an asymmetric spacing around that particle, triggering a dynamics that drives the train to recover its

original spacing s_1. Indeed, the repulsion between slightly closer particles at $s_1 - \epsilon$ is stronger than that between the more distant ones at $s_1 + \epsilon$ [see Fig. 4(b) and its caption]. On the contrary, if the train spacing is smaller than s_{cr}, say, s_2, the reverse dynamics occurs, whereby the closer particles tend to come into contact, forming a doublet [Fig. 4(c)]. Thus, a train with a large spacing (with respect to s_{cr}) is stable, whereas a train with a small spacing is unstable and might develop particle pairing. Particle ordering and particle pairing naturally stem from the stability analysis.

The dimensionless train spacing s^* is, of course, linked to the actual volume fraction used in the experiments, by the purely geometrical relation [40]

$$s^*\phi = \phi_{mp}\beta^2, \tag{2}$$

where ϕ_{mp} is the maximum packing with spherical particles inscribed in the channel. In the case of a square channel, $\phi_{mp} = \pi/6$. Thus, large train spacings, i.e., volume fractions smaller than $\phi_{cr} = \phi_{mp}\beta^2/s^*_{cr}$, promote particle trains ("ordering"), whereas small spacings induce particle "pairing" within the train. Notice that, as mentioned above, Eq. (2) is derived by geometrical considerations. Hence, the train spacing s^* does not depend on the fluid rheology. On the other hand, the shape of the force vs. particle distance curve in Fig. 4(a) and the critical value s^*_{cr} are affected by the rheological properties of the suspending fluid. For instance, at lower Deborah numbers, the force becomes attractive at small interparticle distances [29], promoting doublet formation. Higher viscosities of a Newtonian solvent move s^*_{cr} toward lower values, although the force magnitude is reduced [29], delaying the ordering dynamics. However, a systematic investigation of the effect of fluid rheology on the shape of the pairwise force as well as the physical arguments leading to such force are still lacking, which will be part of the future work.

The results of this simple analysis do correspond to both our experimental observations and numerical predictions. In view of this agreement, we can conclude that viscoelasticity enters the train stability scenario only through the "shape" of the repulsive pairwise force and modulates the kinetics of train formation when it occurs. Furthermore, the experimentally observed importance of the shear-thinning behavior of the viscoelastic liquid is confirmed within this heuristic analysis, as the $De > De_{cr}$ condition, giving the qualitative force-spacing scenario of Fig. 4(a), corresponds to shear-thinning conditions.

In light of the simple stability analysis, particle pairing can be drastically reduced by employing particle concentrations lower than ϕ_{cr}. This is very important for applications in flow cytometry and encapsulation, where particle or cell pairing is detrimental. We also anticipate that fluids with different elastic properties will lead to a different shape of the repulsive force curve, providing an additional degree of freedom to prevent particle or cell pairing.

IV. CONCLUSIONS AND PERSPECTIVES

In this work, we discover that fluid viscoelasticity drives self-assembly of particle trains along the centerline of a straight microfluidic channel. In our experiments, particles with diameter $d = 20$ μm first align at the channel centerline of a square-shaped glass microchannel with height $H = 100$ μm and then self-order, forming trains with a throughput up to 2400 particles/s. Particle trains in viscoelastic liquids are thus easily formed, without the need to design complex microfluidic platforms or to use external control systems.

Our results show that shear-thinning of the suspending liquid is required to achieve the ordering. We find good qualitative agreement between experiments and numerical simulations. We also find that the predominant distance between ordered particles does not depend on the Deborah number De or on the distance from the inlet L_z/H. On the other hand, an increase of De and L_z/H enhances the fraction of ordered particles. As loading increases, particle ordering is somehow perturbed by the formation of particle pairs.

Experimental and numerical evidence can be justified by a simple stability analysis, based on the presence of an effective peculiar repulsive potential between particles. In channel flows, this "repulsive field," which stems from hydrodynamic interactions in viscoelastic liquids at large De, promotes either particle ordering or particle pairing. This picture is indeed very intriguing and might be of larger generality: as in other situations [49,50], self-assembly can come out from repulsion in geometrically constrained situations, like our 1D caging at the channel centerline. From the same stability argument, we learn that particle pairing, which is detrimental in applications related to flow cytometry and encapsulation, can be avoided by tuning the fluid rheology and particle concentration. Therefore, testing the effect of different viscoelastic shear-thinning liquids and particle concentrations on the train formation is worthy of investigation.

The present results can be applied to biomedical engineering and material science. For instance, ordering of biological objects at the channel centerline would be beneficial for optimized flow cytometry [1,3] and deterministic cell encapsulation [5,6]. In high-throughput flow cytometry, for instance, ordering may prevent cells from overlapping at large cell loadings, which is commonly observed in elastic constant-viscosity liquids [Fig. 2(c)]. A constant spacing between particles is also beneficial for the real-time analysis of flowing cells, since it reduces computational costs associated with data analysis [18]. Shear-thinning fluids display an almost flat velocity profile near the channel centerline at $De > 1$; thus, flowing cells can be potentially undeformed (or only slightly deformed), which is optimal for the manipulation of delicate cells [32]. Furthermore, as compared to inertial microfluidics,

the relatively low flow rates needed to achieve ordering are more compatible with downstream droplet generation systems. In material science, our results may prompt further efforts toward microfluidic fabrication of materials to enhance localized properties at the micrometer-size level [51–54]. Techniques such as the "Stokes trap" [55] can be employed to further understand hydrodynamic particle-particle interactions in viscoelastic liquids.

ACKNOWLEDGMENTS

F.D.G. and A.Q.S. gratefully acknowledge the support of the Okinawa Institute of Science and Technology Graduate University with subsidy funding from the Cabinet Office, Government of Japan. A.Q.S. also acknowledges funding from the Japan Society for the Promotion of Science (Grants-in-Aid for Scientific Research (B), Grant No. 18H01135) and Grants-in-Aid for Scientific Research (C), Grant No. 17K06173).

[1] John Oakey, Robert W. Applegate, Jr., Erik Arellano, Dino Di Carlo, Steven W. Graves, and Mehmet Toner, Particle focusing in staged inertial microfluidic devices for flow cytometry, Anal. Chem. **82**, 3862 (2010).

[2] David Erickson and Dongqing Li, Integrated microfluidic devices, Anal. Chimi. Acta **507**, 11 (2004).

[3] Soojung Claire Hur, Henry Tat Kwong Tse, and Dino Di Carlo, Sheathless inertial cell ordering for extreme throughput flow cytometry, Lab Chip **10**, 274 (2010).

[4] Daniel R. Gossett, Westbrook M. Weaver, Albert J. Mach, Soojung Claire Hur, Henry Tat Kwong Tse, Wonhee Lee, Hamed Amini, and Dino Di Carlo, Label-free cell separation and sorting in microfluidic systems, Anal. Bioanal. Chem. **397**, 3249 (2010).

[5] Jon F. Edd, Dino Di Carlo, Katherine J. Humphry, Sarah Köster, Daniel Irimia, David A. Weitz, and Mehmet Toner, Controlled encapsulation of single-cells into monodisperse picolitre drops, Lab Chip **8**, 1262 (2008).

[6] Evelien W. M. Kemna, Rogier M. Schoeman, Floor Wolbers, Istvan Vermes, David A. Weitz, and Albert Van Den Berg, High-yield cell ordering and deterministic cell-in-droplet encapsulation using dean flow in a curved microchannel, Lab Chip **12**, 2881 (2012).

[7] Wonhee Lee, Hamed Amini, Howard A. Stone, and Dino Di Carlo, Dynamic self-assembly and control of microfluidic particle crystals, Proc. Nat. Acad. Sci. **107**, 22413 (2010).

[8] James E. Hallett, Francesco Turci, and C. Patrick Royall, Local structure in deeply supercooled liquids exhibits growing lengthscales and dynamical correlations, Nat. Commun. **9**, 3272 (2018).

[9] Juan Luis Aragones, Joshua Paul Steimel, and Alfredo Alexander Katz, Elasticity-induced force reversal between active spinning particles in dense passive media, Nat. Commun. **7**, 11325 (2016).

[10] Kevin A. Arpin, Agustin Mihi, Harley T. Johnson, Alfred J. Baca, John A. Rogers, Jennifer A. Lewis, and Paul V. Braun, Multidimensional architectures for functional optical devices, Adv. Mater. **22**, 1084 (2010).

[11] Pai Wang, Filippo Casadei, Sicong Shan, James C. Weaver, and Katia Bertoldi, Harnessing Buckling to Design Tunable Locally Resonant Acoustic Metamaterials, Phys. Rev. Lett. **113**, 014301 (2014).

[12] Scott J. Hollister, Porous scaffold design for tissue engineering, Nat. Mater. **4**, 518 (2005).

[13] Paul Calvert, Printing cells, Sciences **318**, 208 (2007).

[14] G. Segre and Alex Silberberg, Behaviour of macroscopic rigid spheres in poiseuille flow part 2, experimental results and interpretation, J. Fluid Mech. **14**, 136 (1962).

[15] Jean-Philippe Matas and Virginie Glezer, Trains of particles in finite-Reynolds-Number pipe flow, Phys. Fluids **16**, 4192 (2004).

[16] Dino Di Carlo, Daniel Irimia, Ronald G. Tompkins, and Mehmet Toner, Continuous inertial focusing, ordering, and separation of particles in microchannels, Proce. Nat. Acad. Sci. **104**, 18892 (2007).

[17] Jeong-Ah Kim, J. Lee, Chue-Yu Wu, S. Nam, Dino Di Carlo, and Wonhee Lee, Inertial focusing in non-rectangular cross-section microchannels and manipulation of accessible focusing positions, Lab Chip **16**, 992 (2016).

[18] Keisuke Goda, Ali Ayazi, Daniel R. Gossett, Jagannath Sadasivam, Cejo K. Lonappan, Elodie Sollier, AliM Fard, Soojung Claire Hur, Jost Adam, Coleman Murray, and C. Wang, High-throughput single-microparticle imaging flow analyzer, Proc. Nat. Acad. Sci. **109**, 11630 (2012).

[19] Gaetano D'Avino, Giovanni Romeo, Massimiliano M. Villone, Francesco Greco, Paolo A. Netti, and Pier Luca Maffettone, Single line particle focusing induced by viscoelasticity of the suspending liquid: Theory, experiments and simulations to design a micropipe flow-focuser, Lab Chip **12**, 1638 (2012).

[20] Seungyoung Yang, Jae Young Kim, Seong Jae Lee, Sung Sik Lee, and Ju Min Kim, Sheathless elasto-inertial particle focusing and continuous separation in a straight rectangular microchannel, Lab Chip **11**, 266 (2011).

[21] Ilaria De Santo, Gaetano D'Avino, Giovanni Romeo, Francesco Greco, Paolo A. Netti, and Pier Luca Maffettone, Microfluidic Lagrangian Trap for Brownian Particles: Three-Dimensional Focusing Down to the Nanoscale, Phys. Rev. Appl. **2**, 064001 (2014).

[22] Alex M. Leshansky, Avishay Bransky, Netanel Korin, and Uri Dinnar, Tunable Nonlinear Viscoelastic Focusing in a Microfluidic Device, Phys. Rev. Lett. **98**, 234501 (2007).

[23] Gaetano D'Avino, Francesco Greco, and Pier Luca Maffettone, Particle migration due to viscoelasticity of the suspending liquid and its relevance in microfluidic devices, Ann. Rev. Fluid Mech. **49**, 341 (2017).

[24] Xinyu Lu, Chao Liu, Guoqing Hu, and Xiangchun Xuan, Particle manipulations in non-newtonian microfluidics: A review, J. Colloid Interface Sci. **500**, 182 (2017).

[25] Dan Yuan, Qianbin Zhao, Sheng Yan, Shi-Yang Tang, Gursel Alici, Jun Zhang, and Weihua Li, Recent progress of particle migration in viscoelastic fluids, Lab Chip **18**, 551 (2018).

[26] Nan Xiang, Xinjie Zhang, Qing Dai, Jie Cheng, Ke Chen, and Zhonghua Ni, Fundamentals of elasto-inertial particle focusing in curved microfluidic channels, Lab Chip **16**, 2626 (2016).

[27] Nan Xiang, Zhonghua Ni, and Hong Yi, Concentration-controlled particle focusing in spiral elasto-inertial microfluidic devices, Electrophoresis **39**, 417 (2018).

[28] Ah Reum Kang, Sung Won Ahn, Seong Jae Lee, Byunghwan Lee, Sung Sik Lee, and JuMin Kim, Medium viscoelastic effect on particle segregation in concentrated suspensions under rectangular microchannel flows, Korea-Australia Rheol. J. **23**, 247 (2011).

[29] Gaetano D'Avino, Martin A. Hulsen, and Pier Luca Maffettone, Dynamics of pairs and triplets of particles in a viscoelastic fluid flowing in a cylindrical channel, Comput. Fluids. **86**, 45 (2013).

[30] Francesco Del Giudice, Gaetano D'Avino, Francesco Greco, Paolo A. Netti, and Pier Luca Maffettone, Effect of fluid rheology on particle migration in a square-shaped microchannel, Microfluidics Nanofluidics **19**, 95 (2015).

[31] Di Li and Xiangchun Xuan, Fluid rheological effects on particle migration in a straight rectangular microchannel, Microfluidics Nanofluidics **22**, 49 (2018).

[32] Francesco Del Giudice, Shivani Sathish, Gaetano D'Avino, and Amy Q. Shen, "From the edge to the center": Viscoelastic migration of particles and cells in a strongly shear-thinning liquid flowing in a microchannel, Anal. Chem. **89**, 13146 (2017).

[33] David J. Guckenberger, Theodorus E. de Groot, Alwin M. D. Wan, David J. Beebe, and Edmond W. K. Young, Micromilling: A method for ultra-rapid prototyping of plastic microfluidic devices, Lab Chip **15**, 2364 (2015).

[34] John C. Crocker and David G. Grier, Methods of digital video microscopy for colloidal studies, J. Colloid Interface Sci. **179**, 298 (1996).

[35] Christopher W. Macosko and Ronald G. Larson, *Rheology: Principles, measurements, and applications* (VCH, New York, 1994).

[36] Francesco Del Giudice, Francesco Greco, Paolo Antonio Netti, and Pier Luca Maffettone, Is microrheometry affected by channel deformation? Biomicrofluidics **10**, 043501 (2016).

[37] Gaetano D'Avino and Pier Luca Maffettone, Particle dynamics in viscoelastic liquids, J. Non-Newtonian Fluid Mech. **215**, 80 (2015).

[38] Soroush Kahkeshani, Hamed Haddadi, and Dino Di Carlo, Preferred interparticle spacings in trains of particles in inertial microchannel flows, J. Fluid Mech. **786**, (2016).

[39] Katherine J. Humphry, Pandurang M. Kulkarni, David A. Weitz, Jeffrey F. Morris, and Howard A. Stone, Axial and lateral particle ordering in finite Reynolds Number channel flows, Phys. Fluids **22**, 081703 (2010).

[40] See supplemental material at http://link.aps.org/supplemental/10.1103/PhysRevApplied.10.064058 for details on the injection policy, more details on the adopted procedure, the validity of the assumptions and the validation. The full derivation of Eq. 2 is also reported.

[41] Ronald G. Larson, *Constitutive Equations for Polymer Melts and Solutions* (Butterworth-Heinemann, Boston, 2013).

[42] Arjen C. B. Bogaerds, Anne M. Grillet, Gerrit W. M. Peters, and Frank P. T. Baaijens, Stability analysis of polymer shear flows using the extended pom–pom constitutive equations, J. Non-Newtonian Fluid Mech. **108**, 187 (2002).

[43] Robert Guénette and Michel Fortin, A new mixed finite element method for computing viscoelastic flows, J. Non-Newtonian Fluid Mech. **60**, 27 (1995).

[44] Alexander N. Brooks and Thomas J. R. Hughes, Streamline upwind/petrov-galerkin formulations for convection dominated flows with particular emphasis on the incompressible navier-stokes equations, Comput. Methods Appl. Mech. Eng. **32**, 199 (1982).

[45] Raanan Fattal and Raz Kupferman, Constitutive laws for the matrix-logarithm of the conformation tensor, J. Non-Newtonian Fluid Mech. **123**, 281 (2004).

[46] Martien A. Hulsen, Raanan Fattal, and Raz Kupferman, Flow of viscoelastic fluids past a cylinder at high weissenberg number: Stabilized simulations using matrix logarithms, J. Non-Newtonian Fluid Mech. **127**, 27 (2005).

[47] Howard H. Hu, Neelesh A. Patankar, and M. Y. Zhu, Direct numerical simulations of fluid–solid systems using the arbitrary lagrangian–eulerian technique, J. Comput. Phys. **169**, 427 (2001).

[48] Arjen C. B. Bogaerds, Martien A. Hulsen, Gerrit W. M. Peters, and Frank P. T. Baaijens, Stability analysis of injection molding flows, J. Rheol. **48**, 765 (2004).

[49] Pawel Pieranski, Two-Dimensional Interfacial Colloidal Crystals, Phys. Rev. Lett. **45**, 569 (1980).

[50] Duck-Gyu Lee, Pietro Cicuta, and Dominic Vella, Self-assembly of repulsive interfacial particles via collective sinking, Soft Matter **13**, 212 (2017).

[51] Kevin S. Paulsen, Dino Di Carlo, and Aram J. Chung, Optofluidic fabrication for 3d-shaped particles, Nat. Commun. **6**, (2015).

[52] Bing Xu, Yang Shi, Zhao-Xin Lao, Jin-Cheng Ni, Guoqiang Li, Yanlei Hu, Jiawen Li, Jia-ru Chu, Dong Wu, and Koji Sugioka, Real-time two-photon-lithography in controlled flow to create a single-microparticle-array and particle-cluster-array for optofluidic imaging, Lab Chip **18**, 442 (2017).

[53] Qibin Zhao, Chris E. Finlayson, David R. E. Snoswell, Andrew Haines, Christian Schäfer, Peter Spahn, Goetz P. Hellmann, Andrei V. Petukhov, Lars Herrmann, Pierre Burdet, and P. A. Midgley, Large-scale ordering of nanoparticles using viscoelastic shear processing, Nat. Commun. **7**, 11661 (2016).

[54] Sagar Yadavali, Heon-Ho Jeong, Daeyeon Lee, and David Issadore, Silicon and glass very large scale microfluidic droplet integration for terascale generation of polymer microparticles, Nat. Commun. **9**, 1222 (2018).

[55] Anish Shenoy, Christopher V. Rao, and Charles M. Schroeder, Stokes trap for multiplexed particle manipulation and assembly using fluidics, Proc. Nat. Acad. Sci. **113**, 201525162 (2016).